Article

Characterization of Three-Dimensional Internal Structure Evolution in Asphalt Mixtures during Freeze–Thaw Cycles

Gang Xu *, Xianhua Chen [ID]**, Xing Cai, Yunhong Yu and Jun Yang**

School of Transportation, Southeast University, 2 Sipailou, Nanjing 210096, China; chenxh@seu.edu.cn (X.C.); tsing2017@seu.edu.cn (X.C.); yyh@seu.edu.cn (Y.Y.); yangjun@seu.edu.cn (J.Y.)
* Correspondence: 220162683@seu.edu.cn

Abstract: This paper aims to characterize the three-dimensional (3D) internal structure evolution of asphalt mixtures under freeze–thaw cycles. Asphalt mixtures with three levels of design void content (3%, 5%, and 7%) were prepared in the laboratory. Subsequently, X-ray computed tomography (CT) tests were conducted to capture two-dimensional (2D) images of the internal structure of samples before and after freeze–thaw testing. A set of image processing techniques for reconstructing 3D images of the internal structure were utilized to extract the internal structure properties, which were then used to analyze the changes in the air void distributions and to evaluate the internal structure evolution under freeze–thaw cycles. 3D images reconstructed from X-ray CT images illustrated a dramatic degradation in the internal structure after cyclic freeze–thaw exposure. The change in internal structure occurs mainly in three ways: (1) expansion of existing individual voids, (2) combination of two separated air voids, and (3) generation of new voids. In addition, the parametric analysis of the three-dimensional reconstructed voids revealed that the asphalt mixture void ratio increased with the number of freeze–thaw cycles, while the larger the initial void content, the more pronounced the increase in the specimens. Therefore, asphalt mixture freeze–thaw resistance should be optimized in relation to the design void content.

Keywords: asphalt mixtures; X-ray computed tomography; 3D internal structure; freeze–thaw cycles; design void content

1. Introduction

Waterproofing layers are essential to prevent surface water from infiltrating into the high-speed railway subgrade to ensure its stability and bearing capacity, especially in the seasonally frozen regions to prevent subgrade frost [1–4]. The dense-graded asphalt concrete was used as a waterproofing material to substitute for fiber-reinforced concrete. Its requirements are proposed based on the practice achievements in Beijing–Zhangjiakou high-speed railway test section [5–7].

However, a systematic approach to asphalt mixture waterproofing layer system design in high-speed railway system has not been formed, which will limit its widespread use. Air void content is an important parameter in asphalt mixtures, as it has great influence on their permeability and durability. Practicing engineers have suggested that the air void should not exceed 5% based on road construction experience in highway engineering. This is not a scientific conclusion, since there are significant differences between waterproofing layers and road pavements. The waterproofing layer aims to prevent water infiltration and previous field tests have proven that the bearing capacity does not need to be considered [8]. Asphalt mixture is a composite material comprising voids, aggregates, fillers, and asphalt binder. The internal structure of asphalt mixtures is sensitive to freeze–thaw cycles, resulting in an increased permeability and subsequent damage to the subgrade, especially in cold regions [9]. Therefore, in order to guide asphalt mixture waterproofing layer design in cold regions, the evolution of internal structure inside asphalt mixture exposed to freeze–thaw cycles should be explored first.

Mohammad et al. proved that specimens with the same macro-scale air void volume may have diverse aggregate and air void distributions, resulting in distinct performance behavior under freeze–thaw cycles [10,11]. X-ray CT is a useful advanced technology that allows porous media to be characterized on the basis of their micro–level structure distribution. X-ray CT requires no sample treatment before scanning and is non-destructive to the sample for further experiments, which is essential for studying the evolution of internal structure before and after freeze–thaw cycles [12,13].

Researchers have conducted numerous studies to characterize the internal structure of asphalt mixtures via 2D and 3D imaging, for specific types of asphalt mixture. They used image analysis to evaluate orientation of the aggregate particles, aggregate gradation, and air void distribution [14–17]. Al-Omari et al. [18] studied the relationship between the permeability of asphalt mixture and 3D distribution of voids. They quantitatively analyzed the effect of irregular flow paths, effective void fraction, and void surface areas on permeability by using a modified Kozeny–Carman equation. Moreover, the internal structure of asphalt mixtures under mechanical loading was also evaluated by various researchers. Wang et al. [19] defined three parameters to describe the spatial distribution of voids in order to characterize the internal structural damage of asphalt mixtures and quantitatively analyze void content and void size. Khan et al. employed void parameters, including void content and void connectivity, to characterize the moisture content and saturation of asphalt mixtures. The authors correlated these parameters with the relative stiffness obtained from mechanical testing to demonstrate the negative effect of moisture on the performance of asphalt mixtures [20,21]. Meanwhile, Xu et al. [9] reported that the effect of design of air voids and water saturation on the internal structure evolution of asphalt mixtures before and after freeze–thaw cycles was not negligible. They found out that low air void content and air voids in partially saturated asphalt mixtures possessed strong resistance to freeze–thaw damage.

It can be summarized that previous efforts by researchers for the analysis of internal structure of asphalt mixtures using X-ray CT images mainly relied on 2D images before and after freeze–thaw cycles. Not much emphasis was given to the 3D internal structure evolution during freeze–thaw processes, which could provide more intuitive evidence for the performance deterioration under environmental loading in cold regions. Therefore, the air void content of dense-graded asphalt mixtures was considered in the present experimental study. Sampled asphalt mixtures were scanned before freeze–thaw testing to characterize their initial internal structure. Thereafter, cylindrical compacted specimens were subjected to freeze–thaw cycles. After 5, 15, 25, and 35 cycles, damaged asphalt mixture specimens were collected for X-ray CT to identify the changes in internal structure. Changes in the 3D internal structure, which was constructed by 2D images after 3D reconstruction, were used to evaluate the effect of freeze–thaw exposure on the internal structure evolution of asphalt mixtures.

2. Material and Methods

2.1. Specimen Preparation and Testing

In this research, three levels of air void content (3%, 5%, and 7%) of dense-graded asphalt mixtures (AC) with 5% SBS/CR compound modified asphalt were used, which was provided by Jiangsu Baoli International Investment Co., Ltd., China, and its properties were shown in Table 1. The AC contains 40 percent coarse aggregate with a nominal maximum aggregate size of 16 mm. All asphalt mixtures were specified based on Technical Specifications for Construction of Highway Asphalt Pavements in China (JTG F40-2004). The specimen was compacted by using a gyratory compactor in height control, with 0.6 MPa vertical pressure, angle of gyration at 1.25°, and 30 rpm gyration speed. Details of the mix design, designed air void content, and freeze–thaw test conditions are shown in Figure 1 and Table 2.

Table 1. Properties of bitumen.

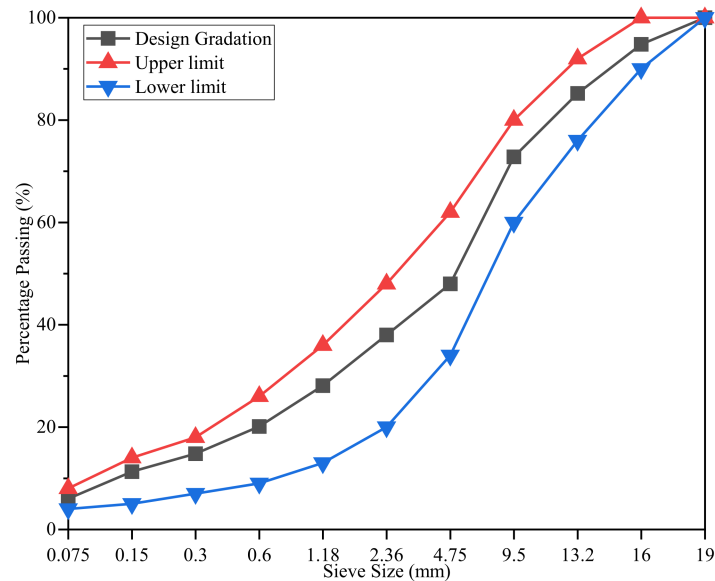| Properties	Unit	Test Results	Test Method
Penetration (25 °C, 100 g, 5 s)	(0.1 mm)	68.9	ASTM D5
Softening point (ring and ball method)	°C	87.2	ASTM D36
Ductility (5 °C, 5 cm/s)	cm	43	ASTM D113
Change in mass TFOT	%	−0.2	ASTM D2872
Flashpoint, Cleveland open cup	°C	289	ASTM D92

Figure 1. Aggregate gradation curves of AC 16.

Table 2. Details of specimens for freeze–thaw tests.

Freeze–Thaw Test Detail			Air Void Content/%	Gyration Numbers
Step 1: Water conditioned by Vacuum saturation using a residual pressure of 98 kPa for 15 min	Step 2-1: Freezing in the air at −5 °C for 12 h	Thawing in the water at 25 °C for 6 h	3.10	180
	Step 2-2: Freezing in the air at −15 °C for 4 h		5.05	126
	Step 2-3: Freezing in the air at −25 °C for 2 h		7.12	80

To simulate the climatic field conditions, the climate data in Zhangjiakou from China Meteorological Administration were obtained. The days of a temperature that had the average temperature in a day occurred in the past five years were calculated, and obtained the proportion of the days of per average temperature to the total days was obtained. Next, the normal fitting method was used to fit the data of average temperature-proportion, which is shown in Figure 2. Finally, the enclosed area ratio between the curve and horizontal axis of −30 and −20 °C, −20 and −10 °C, and −10 and 0 °C was calculated by MATLAB. Therefore, in a freeze–thaw cycle, firstly, all the specimens were conditioned in the distilled water by vacuum saturation using a residual pressure of 98 kPa for 15 min. Afterwards, specimens were immersed in a container filled with distilled water for 2 h and then frozen in a refrigerator at a temperature of −5 °C for 12 h, followed by −15 °C for 4 h and −25 °C for 2 h. Finally, the specimens were thawed in water at 25 °C for 6 h. Asphalt mixture samples were scanned before freeze–thaw testing to determine the initial internal structure characteristics. The specimens were then subjected to 35 successive freeze–thaw

cycles under the same conditions. After 5, 15, 25, and 35 freeze–thaw cycles, damaged asphalt mixture specimens were collected for X-ray CT testing to identify changes in the internal structure.
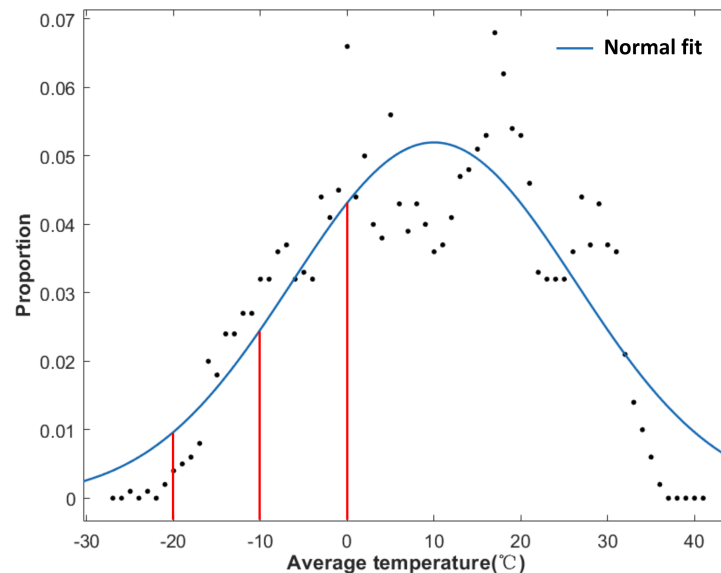

Figure 2. Normal fitting of average temperature-proportion.

2.2. X-ray Scanning and Digital Image Processing

Parameters such as air void content, air void number, and average void diameter have been successfully utilized in characterizing the internal structure of asphalt mixtures. These parameters were well established and verified in previous work [16,22,23]. However, previous researchers relied on obtaining these parameters from two-dimensional digital image slices, limiting the extent to which the development of damage by freeze–thaw can be detected. This also holds true in cases where the variations in internal structural properties were determined along the height (vertical direction) of the specimens. Considering that the internal structure evolution of asphalt mixture by freeze-damage occurs in three dimensions and without a determined direction, it is necessary to use three-dimensional parameters to characterize the internal structure evolution of asphalt mixture during freeze–thaw cycles. In this paper, the internal structure evolution of samples were characterized by their air void content, air void number, and average void diameter in 3D via image processing, as shown in Figure 3; more details can be found in my previous research [24]. For a precise characterization of the internal structure, samples were scanned before and after freeze–thaw exposure to evaluate the changes in their internal structure with a vertical interval of 0.1 mm along the height of the specimens and with a system resolution of 0.05 mm/pixel. The core sample with a diameter of 50 mm and a height of 90 mm was drilled from the surface of the specimen prepared in the gyratory compactor. In addition, the algorithm of Yan [25] was employed to calculate the air voids' volumetric fractals, which are an effective parameter to describe the evolution of void shape during freeze–thaw cycles.

Voids' volumetric fractals are a significant parameter to quantify the complexity of void shape caused by the new micro-cracks and micro-voids during freeze–thaw cycles. When the air voids had been reconstructed by MATLAB toolbox, then 26 neighborhoods shown in Figure 4 were taken to discriminate each void and the voids were numbered by the image processing procedure shown in Figure 3, and the voxel of each void was read out. Subsequently, as each voxel represents $0.05 \times 0.05 \times 0.05$ mm, the volume of each void was calculated, and all results about air void could be output from Matlab toolbox, as shown in Table 3. Finally, the total void volume was obtained by accumulating the volume of each void, and the total volume of the specimen was identified by the procedure. Meanwhile, the equivalent diameter was calculated for each irregularly shaped void volume as a regularly

shaped sphere. The 3D void content and average void diameter were calculated by using Equations (1) and (2), where V_{Total} corresponds to the sum of all voids' volume.
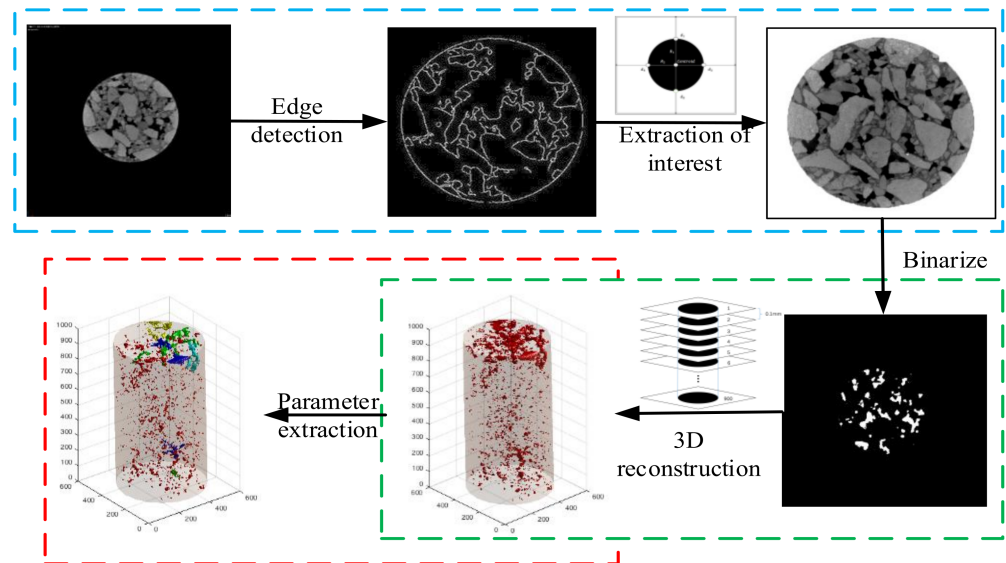

Figure 3. Imaging processing technique [24].

$$Air\ voids\ content(\%) = \frac{V_{Total}}{Total\ specimens\ volume} \times 100 \tag{1}$$

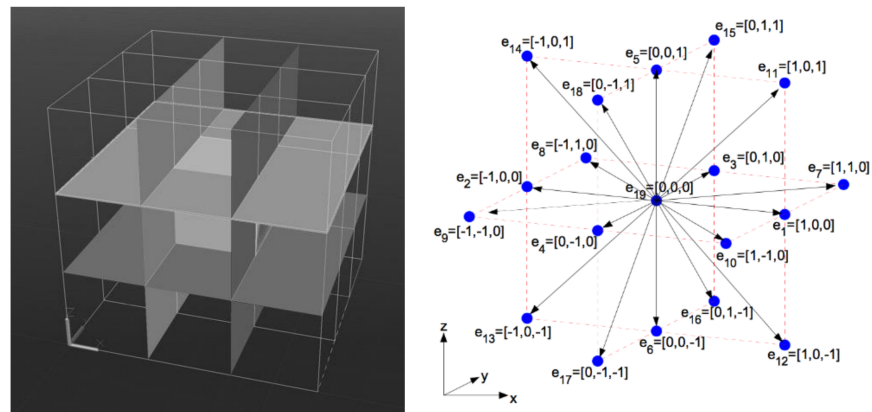$$Average\ voids\ diameter = 2 \times \sqrt[3]{\frac{3V_{Total}}{4\pi}} \tag{2}$$

Figure 4. Principle of the three-dimensional 26-neighborhood division of connected domains.

The voids' volumetric fractals need a specific algorithm based on Equations (3) and (4). Firstly, using a series of cubes with a length of 32 to 1 to cover the 3D void model, the relationship between length (ε) and number($N(\varepsilon)$) was established, as shown in Equation (3). Then, the form of Equation (3) was changed to Equation (4), and a linear function was used to fit the relationship between lgε and lg($N(\varepsilon)$). The absolute value of the slope of linear function is the voids' volumetric fractals.

$$N(\varepsilon) = k\varepsilon^{-D} \tag{3}$$

$$\lg N(\varepsilon) = \lg k - D\lg\varepsilon \tag{4}$$

Results of selected specimens' air void content were obtained via image processing and compared with the laboratory test data, as shown in Table 4. It must be noted that the designable air void content is for specimens before drilling, whereas the measured and simulated air void content correspond to core samples. The disparity of designable and measured air void is clear, especially for specimens that had been designed at 3% air void content. This phenomenon was caused by the uneven distribution of air voids within the specimen prepared in the gyratory compactor. The voids in the central portion were smaller than the surrounding area, and it became more obvious when the degree of compaction increased, as shown in Figure 5. Therefore, the air void content of core samples that were drilled at the surface of the specimen prepared in gyratory compactor was smaller. The air void of core samples designed with 3% air void content could be significantly smaller than the design void content because of excessive compaction [26].

Table 3. Measurement results of air voids.

Void Serial Numbers	X-Direction (pixel)	X-Direction (pixel)	X-Direction (pixel)	Voxel	Volume (mm^3)
1	288	316	333	108,881	13.61
2	151	293	426	88,564	11.07
3	153	254	366	58,811	7.35
4	216	296	333	56,158	7.02
5	344	169	199	41,325	5.16
6	336	263	109	33,808	4.23
⋮	⋮	⋮	⋮	⋮	⋮
5011	2	2	2	8	0.001
5012	2	2	2	8	0.001

Table 4. Laboratory experimented and simulated variables with six combinations.

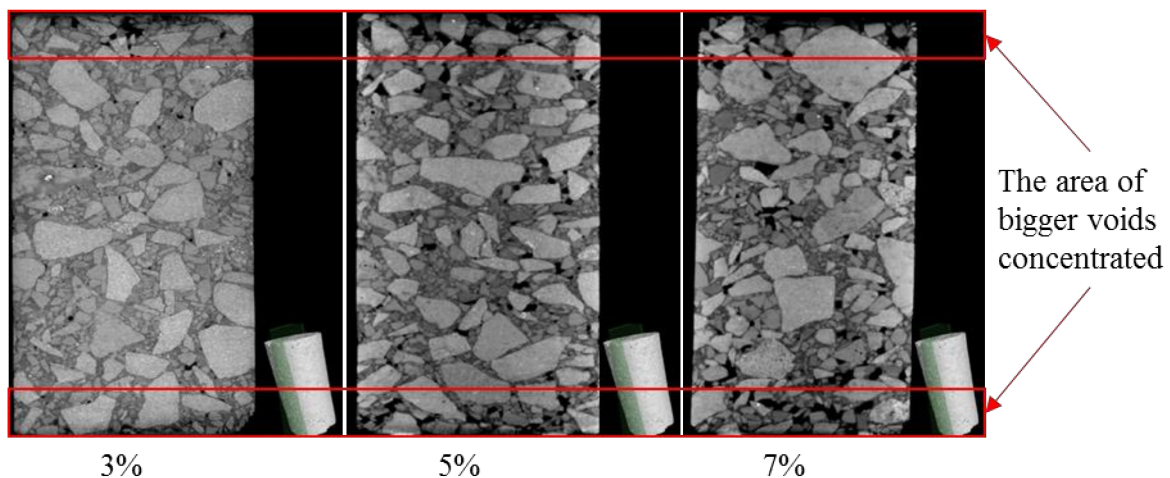| F-T Cycles	0			5		
Designed Voids Content	Experimented	Simulated	Difference	Experimented	Simulated	Difference
3%	1.28	1.05	0.23	1.35	1.14	0.21
5%	4.35	4.26	0.09	5.34	5.27	0.07
7%	6.61	6.53	0.08	7.53	7.48	0.05

Figure 5. Air void distribution of different samples' determined from 2D slices (vertical direction).

Comparison of the difference between measured and simulated results revealed that air voids are underestimated by simulations. Meanwhile, the largest difference was

observed for the sample that had been designed to comprise 3% air void content. This was caused by the cross slices that were used in the image processing, particularly the 20 images at the top and bottom of the sample, as these images were abnormally bright and bluey. When radiation reaches the surface of the test piece, the receiver cannot reply to an abrupt change of ray value, which causes an abnormal CT number [27].

3. Results and Discussion

3.1. Three-Dimensional Distribution of Air Voids in Asphalt Mixture during Freeze–Thaw Testing

3D images of asphalt mixture specimens with air voids before and after freeze–thaw cycles reconstructed via image processing (Figure 3) are provided in Figure 6. A striking difference is observed for specimens with different design air void contents during freeze–thaw cycles. 3D images of samples with a design air void content of 7% are filled with yellow voids (which stands for larger voids with a volume greater than 10 mm^3); contrastingly, such voids only appeared at the top and bottom of 3% design air void content samples. However, all 3D images are similar in larger void sizes, voids present in the top and bottom parts of samples compared with the middle part, indicate similarities to the 2D slices shown in Figure 5. Thus, it increases the credibility of the 3D model. When comparing the 3D images with the same design air void under different freeze–thaw cycles, two main changes of the internal structure can be observed. The first one is the emergence of new red regions generated during freeze–thaw cycles, marked with rectangles in Figure 6. Second regions are marked with ellipses in Figure 5, and those regions are divided into two parts. The solid ellipse indicates air void volume increase during freeze–thaw cycles, and the dotted ellipse relates to the connection between existing air voids. These changes illustrate how freeze–thaw cycles can damage the internal structure of the asphalt mixture in three ways: (1) expansion of individual voids under freeze–thaw cycles, (2) generation of new voids under freeze–thaw cycles, and (3) consolidation of two separated air voids under freeze–thaw cycles.

It must be noted that not all colors can be easily distinguished in 3D images containing air voids, so the volume grades defined in these images are not meticulous. For more specific quantitative research, the voids are divided into micropores (<0.1 mm^3), mesopores (0.1~5 mm^3), and macropores (>5 mm^3), and more details of volume distribution of voids for which the results of different design air void content are shown in Tables 5–7.

3.2. Changes of 3D Void Parameters of Asphalt Mixture during Freeze–Thaw Cycles

3D void content, void number, average diameter, and void volume fractals of samples are employed to quantitatively evaluate the effect of freeze–thaw cycles on the internal structure of asphalt mixtures. All 3D internal structure properties for samples with different design air void contents, tested under freeze–thaw cycles, are shown in Figure 7. Figure 7a shows the void content of samples sharply rising when the design void content changes from 3% to 5%, which later becomes very smooth when the design void content changes from 5% to 7%. It matches well with the changes of reconstructed 3D images of samples with different design void contents, which increases the credibility of the 3D analysis on the internal structure of asphalt mixture during freeze–thaw cycles. Regardless of the air void content of samples, the void content increases with increasing number of freeze–thaw cycles. The magnitude of change under the initial five freeze–thaw cycles is largest, greater than the effect of the subsequent 10 freeze–thaw cycles. Those results indicate that the damage of asphalt mixtures during freeze–thaw cycles and the number of freeze–thaw cycles do not satisfy a linear relationship. It is similar to the loss law of the mechanical properties of asphalt mixtures that the damage variable can be divided into three stages, i.e., fast damage period, stable damage, and damage development period, during freeze–thaw cycles [28]. After 35 freeze–thaw cycles, the void content of the sample with a design air void content of 3% increased from 0.96% to 1.4%, the sample with design air void content of 5% increased from 4.35% to 5.92%, and the sample with design air void content

of 7% increased from 6.61% to 8.31%. This reveals that the sample with higher design void content has a higher risk of damage under freeze–thaw cycles.
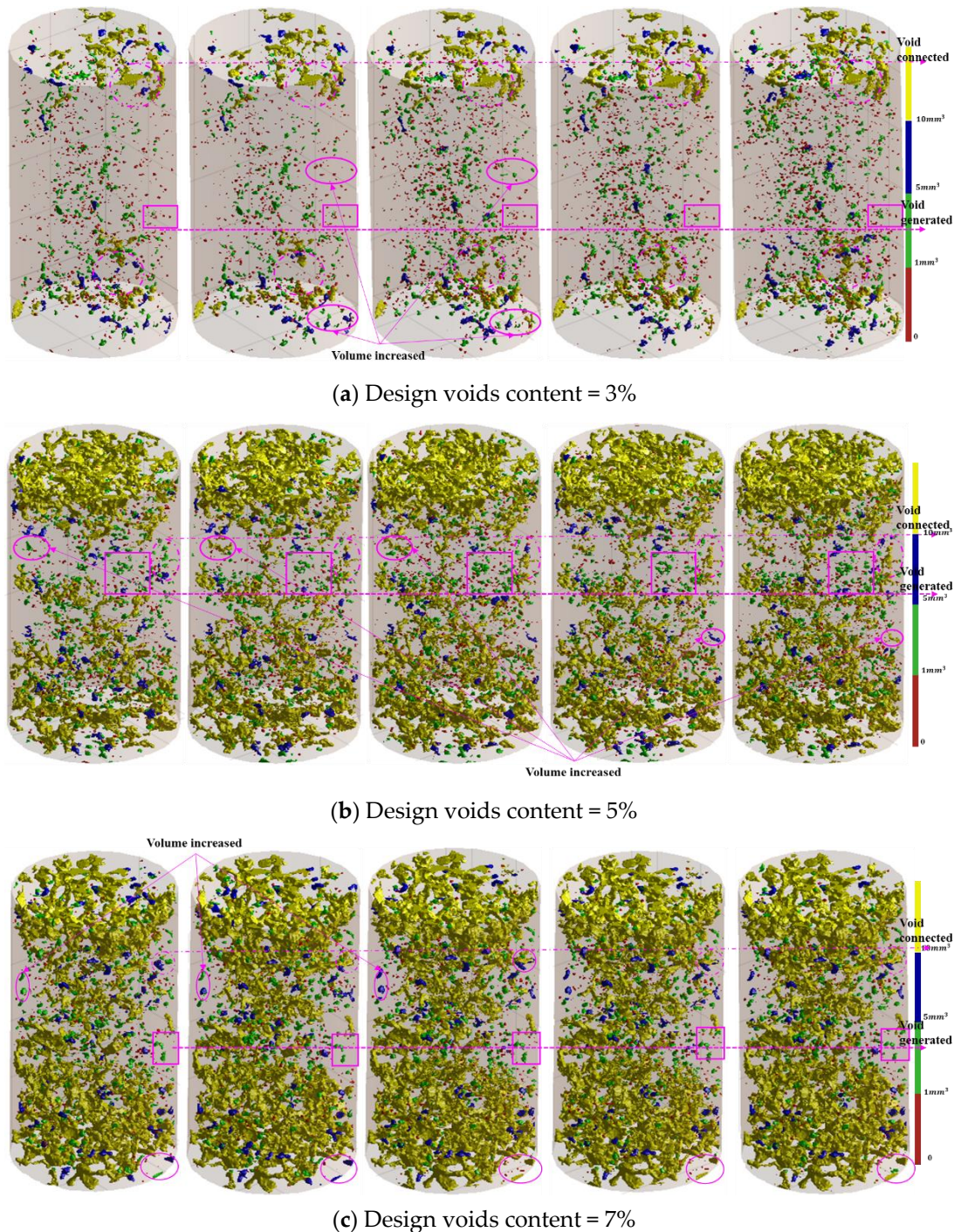

(**a**) Design voids content = 3%

(**b**) Design voids content = 5%

(**c**) Design voids content = 7%

Figure 6. Comparison of air void in 3D of different specimens during freeze–thaw test (from left to right in Figure 5), the 3D air voids images of sample are stand for 0, 5, 15, 25, and 35 freeze–thaw cycles in order).

In Figure 7b, the variation of air void number is not completely consistent with the change of void content. The air void number is not only irregular with the design air void content, but also contains disorder with the number of freeze–thaw cycles. The void number of samples with 3% design void content is the largest, followed by samples with 7% design void content and lastly samples with 5% design void content. It indicates that the void number of samples is not directly related to the design void content. The

formation of voids is random during the progress of sample preparation. Although the void number does not increase with increasing number of freeze–thaw cycles, variation of the air void number is still following a pattern. For example, the air void number of all samples increased their air void content sharply during the initial five freeze–thaw cycles. However, as the number of freeze–thaw cycles reaches 15 or 25, the air void number reduced regardless of the design air void content. Combined with results shown in Table 5, the increase in the air void number of samples under the action of initial five freeze–thaw cycles suggest that the formation of new voids exert a dominant effect to increase the air void content. Consolidation of separated air (new or existing) plays an important role on the effect of air void content with increasing number of freeze–thaw cycles.

Table 5. Design voids content = 3%.

Volume Grades (mm^3)	Number of Freeze–Thaw Cycles				
	0	5	15	25	35
<0.1	2959	4347	3786	3311	3408
0.1~1	1506	1986	1712	1707	1758
1~2	328	349	437	454	467
2~5	243	136	176	214	217
5~10	62	52	77	73	67
10~20	7	8	25	31	28
20~30	1	4	8	6	7
>30	6	10	13	15	15
Total	5112	6892	6234	5811	5967

Table 6. Design voids content = 5%.

Volume Grades (mm^3)	Number of Freeze–Thaw Cycles				
	0	5	15	25	35
<0.1	2031	2758	2119	1803	2003
0.1~1	1206	1686	1722	1573	1517
1~2	528	549	437	586	528
2~5	243	176	236	398	409
5~10	62	55	72	85	80
10~20	17	11	15	19	26
20~30	10	11	16	17	19
>30	6	7	11	13	14
Total	4103	5253	4628	4494	4596

Table 7. Design voids content = 7%.

Volume Grades (mm^3)	Number of Freeze–Thaw Cycles				
	0	5	15	25	35
<0.1	3434	4429	3494	3370	3275
0.1~1	1006	1186	1360	1377	1403
1~2	147	176	337	308	323
2~5	118	125	136	179	208
5~10	50	57	64	85	69
10~20	17	20	25	29	34
20~30	11	11	20	28	20
>30	17	19	24	27	29
Total	4800	6023	5460	5403	5361

(**a**) Voids content

(**b**) Voids number

(**c**) Average voids diameter

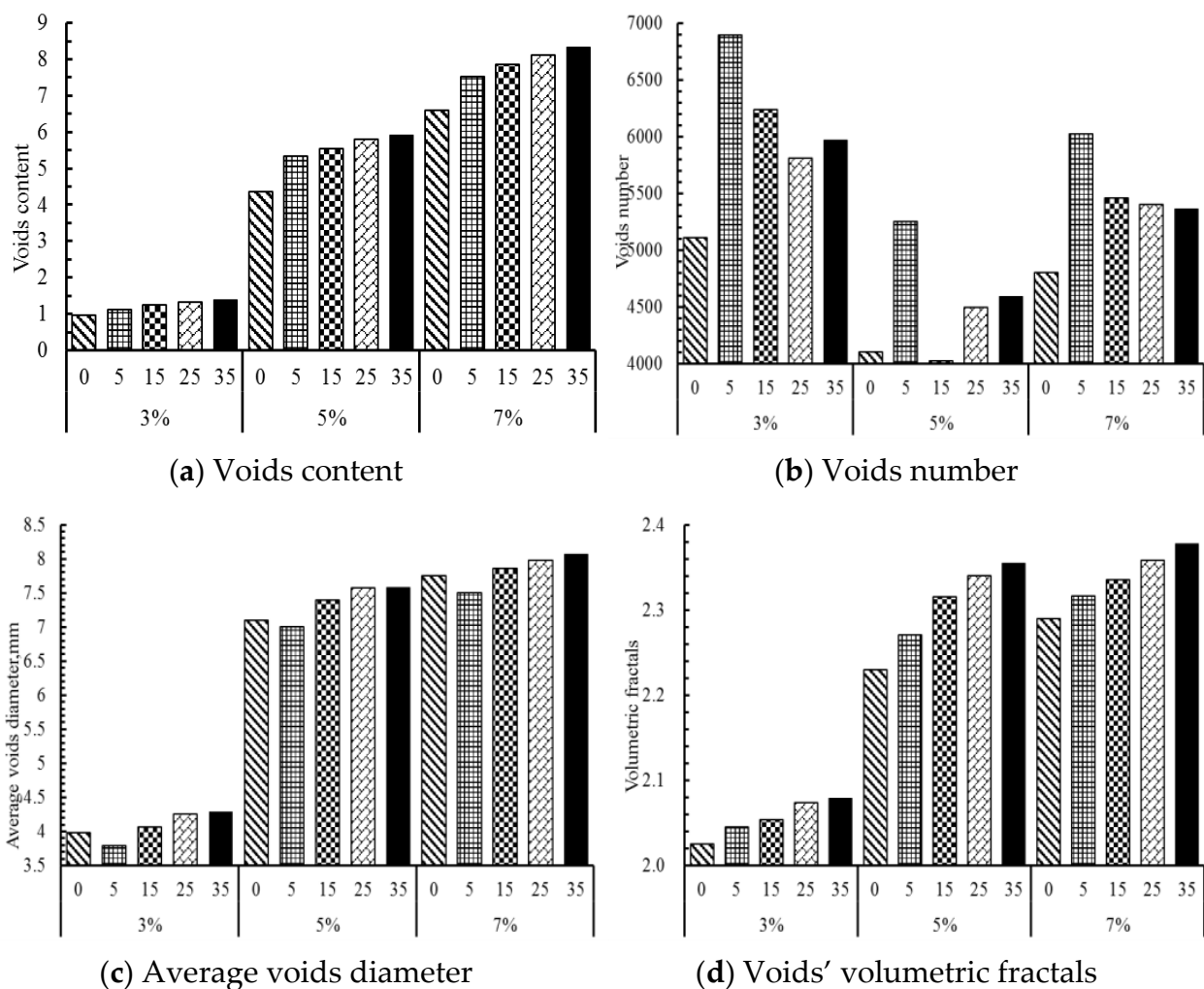(**d**) Voids' volumetric fractals

Figure 7. Effect of design void content on internal structure evolution during freeze–thaw cycles.

Figure 7c shows the changes of average 3D void diameter in asphalt mixtures with three types of design void content, compared before and after freeze–thaw cycles. Average air void diameter abruptly decreases at the initial stages of the test, but gradually increases during the subsequent freeze–thaw cycles regardless of the design void content. As shown in Equation (2), the change of average air void diameter is affected by the variation of void content and void number. Corresponding to the variation in void content, void number, and void volume grades during freeze–thaw cycles, the reduced void diameters in asphalt mixtures at initial stages are caused by increasing number of voids with a volume less than 0.1 mm^3. This demonstrates that it is the newly formed voids that greatly influence the void diameter during freeze–thaw cycles. Moreover, the average void diameter was observed to increase after the fifth freeze–thaw cycle. This result indicates that existing air voids coalesce and air void volume increases with increasing number of freeze–thaw cycles.

Comparing Figure 7a,d, variations of air void content and void volumetric fractals with increasing number of freeze–thaw cycles are investigated. A strong correlation between the air void content and void volumetric fractals in the hot mix asphalt mixture is observed. According to the definition of void volumetric fractals, if the value is closer to 2, its shape approximates a sphere in 3D space. Considering both Figure 7d and Table 4, void volumetric fractals of the sample with design void content of 3% are close to 2, and the majority of air voids' volume is less than 1 mm^3. This demonstrates that void volumetric fractals are related to single void volumes during sample preparation, i.e., the smaller the void volume is, the higher similarity the shape possesses to a sphere. As the air void

content increases, larger voids emerge and hence, void volumetric fractals become larger. However, the volumetric fractals of cracks are not that way; the shape of the crack is very different from the sphere. Therefore, void volumetric fractal is a useful parameter to evaluate the 3D internal structure evolution of asphalt mixture during freeze–thaw cycles. As shown in Figure 7d, void volumetric fractals increase with the increasing number of freeze–thaw cycles, and the growth rate is smooth during the whole freeze–thaw process, yet a difference between samples with different design air void content exists. This result shows that freeze–thaw cycles cause serious damage in the sample via micro-crack formation and propagation under the freeze–thaw action, which is related to the void content. For samples with a smaller void content, the damage of freeze–thaw is smaller, which suggests the design voids content should be smaller than 3% in cold regions.

On the basis of observations on dense-graded asphalt mixtures samples with different design air void contents, it can be concluded that the damage, governed by changes in the 3D internal structure, occurs through various mechanisms that are related to the initial void content. Initial damage is caused by the aggregation of existing voids to form micro-cracks as well as the generation of new voids. After five freeze–thaw cycles, the expansion and connection of newly formed voids play a more dominant role in micro-crack formation than in new void formation. These events increase air void content and void volumetric fractals.

4. Conclusions

Variations in the 3D internal structure of dense-graded asphalt mixtures with three levels of design content under freeze–thaw cycles were identified by capturing X-ray CT images and reconstructing 3D images of voids before and after freeze–thaw testing. The changes in 3D images were utilized to qualitatively analyze the internal structure evolution under the action of freeze–thaw exposure. Meanwhile, void content, void number, and void volumetric fractals were successfully employed to quantify the internal structure evolution associated with deformation under freeze–thaw cycles. Results indicate that the change in internal structure of samples with different design void content mainly occurs in three ways: (1) expansion of individual voids under freeze–thaw cycles, (2) generation of new voids under freeze–thaw cycles, and (3) coalescing of two separated air voids under freeze–thaw cycles. Moreover, the variation of the damage variable can be divided into three stages, i.e., fast damage period, stable damage, and damage development period during freeze–thaw cycles.

Meanwhile, the aforementioned internal structure properties were used to evaluate the influence of the design void content during freeze–thaw cycles. The design void content plays an important role in the study of freeze–thaw damage of asphalt mixtures. Specimens with high design void content tend to propagate micro-cracks and form new voids during freeze–thaw cycling. Therefore, freeze–thaw resistance of asphalt mixtures should be optimized according to the design void content.

References

1. Xue-Ning, M.A.; Liang, B.; Gao, F. Study on the Dynamic Properties of Slab Ballastless Track and Subgrade Structure on High-speed Railway. *J. China Railw. Soc.* **2011**, *33*, 72–78.
2. Yang, J. Research on Design of Waterproof and Drainage for Subgrade of Passenger Dedicated Railway. *J. Railw. Eng. Soc.* **2011**, *28*, 52–55.
3. Zhang, L.T.; Ke, W.U.; Zhang, L.W. Study on Waterproofing and Drainage System for Subgrade of Ballastless Track. *Soil Eng. Found.* **2010**, *31*, 19–24.
4. Zhao, G.; Liu, X.; Gao, L.; Cai, X. Characteristic Analysis of Track Irregularity in Subgrade Frost Heave Area of Harbin-Dalian High-speed Railway. *J. China Railw. Soc.* **2016**, *38*, 105–109.
5. Liu, S.; Yang, J.; Chen, X.; Yang, G.; Cai, D. Application of Mastic Asphalt Waterproofing Layer in High-Speed Railway Track in Cold Regions. *Appl. Sci.* **2018**, *8*, 667. [CrossRef]
6. Liu, S.; Yang, J.; Chen, X.; Wang, M.; Zhou, W. Design of Asphalt Waterproofing Layer for High-Speed Railway Subgrade: A Case Study in Heilongjiang Province, China. In *Transportation Research Board 96th Annual Meeting*; Transportation Research Board: Washington, DC, USA, 2017.
7. Liu, S.; Markine, V.L.; Chen, X.; Yang, J. Numerical Study on Application of Full Cross-Section Asphalt Waterproof Layer in CRTS III Slab Track. In *Transportation Research Board 97th Annual Meeting*; Transportation Research Board: Washington, DC, USA, 2018.
8. Xiahua Chen, T.T.; Yang, G.; Yan, H.; Yang, J. Long-Lasting Waterproofing Solution for the Subgrade of High-Speed Railway in Cold Region. *J. Test. Eval.* **2018**, *47*, 1982–1994.
9. Xu, H.N.; Guo, W.; Tan, Y.Q. Internal structure evolution of asphalt mixtures during freeze-thaw cycles. *Mater. Des.* **2015**, *86*, 436–446. [CrossRef]
10. Mohammad, L.N.; Herath, A.; Huang, B.S.; Trb, T. Evaluation of permeability of Superpave((R)) asphalt mixtures. In *Bituminous Paving Mixtures 2003: Materials and Construction*; Transportation Research Board Natl Research Council: Washington, DC, USA, 2003; pp. 50–58.
11. Hainin, M.R.; Yusoff, N.I.M.; Satar, M.; Brown, E.R. The effect of lift thickness on permeability and the time available for compaction of hot mix asphalt pavement under tropical climate condition. *Constr. Build. Mater.* **2013**, *48*, 315–324. [CrossRef]
12. Nagy, S.; Nosko, M.; Orovcik, L.; Izdinsky, K.; Kudela, S.; Krizik, P. Pre-review study of the aluminum/alumina master alloy made through pressure infiltration. *Mater. Des.* **2015**, *66*, 1–6. [CrossRef]
13. Ibrahim, A.; Zhang, F.M.; Otterstein, E.; Burkel, E. Processing of porous Ti and Ti5Mn foams by spark plasma sintering. *Mater. Des.* **2011**, *32*, 146–153. [CrossRef]
14. Masad, E.; Muhunthan, B.; Shashidhar, N.; Harman, T. Internal structure characterization of asphalt concrete using image analysis. *J. Comput. Civ. Eng.* **1999**, *13*, 88–95. [CrossRef]
15. Kutay, M.E.; Ozturk, H.I.; Abbas, A.R.; Hu, C.C. Comparison of 2D and 3D image-based aggregate morphological indices. *Int. J. Pavement Eng.* **2011**, *12*, 421–431. [CrossRef]
16. Coenen, A.R.; Kutay, M.E.; Sefidmazgi, N.R.; Bahia, H.U. Aggregate structure characterisation of asphalt mixtures using two-dimensional image analysis. *Road Mater. Pavement Des.* **2012**, *13*, 433–454. [CrossRef]
17. Krol, J.B.; Khan, R.; Collop, A.C. The study of the effect of internal structure on permeability of porous asphalt. *Road Mater. Pavement Des.* **2018**, *19*, 935–951. [CrossRef]
18. Al-Omari, A.; Tashman, L.; Masad, E.; Cooley, A.; Harman, T. Proposed methodology for predicting HMA permeability (with discussion). *J. Assoc. Asph. Paving Technol.* **2002**, *71*, 30–58.
19. Wang, L.B.; Wang, X.; Mohammad, L.; Wang, Y.P. Application of mixture theory in the evaluation of mechanical properties of asphalt concrete. *J. Mater. Civ. Eng.* **2004**, *16*, 167–174. [CrossRef]
20. Khan, R.; Collop, A.C.; Airey, G.D.; Khan, A.N. Asphalt damage characterisation from cyclic test and X-ray computed tomography. *Proc. Inst. Civ. Eng. Transp.* **2013**, *166*, 203–213. [CrossRef]
21. Khan, R.; Grenfell, J.; Collop, A.; Airey, G.; Gregory, H. Moisture damage in asphalt mixtures using the modified SATS test and image analysis. *Constr. Build. Mater.* **2013**, *43*, 165–173. [CrossRef]
22. Navaro, J.; Bruneau, D.; Drouadaine, I.; Colin, J.; Dony, A.; Cournet, J. Observation and evaluation of the degree of blending of reclaimed asphalt concretes using microscopy image analysis. *Constr. Build. Mater.* **2012**, *37*, 135–143. [CrossRef]
23. Wu, W.L.; Wang, D.Y.; Zhang, X.N. Estimating the Gradation of Asphalt Mixtures using X-Ray Computerized Tomography and Stereology Method. *Road Mater. Pavement Des.* **2011**, *12*, 699–710. [CrossRef]
24. Xu, G.; Yu, Y.; Cai, D.; Xie, G.; Chen, X.; Yang, J. Multi-scale damage characterization of asphalt mixture subject to freeze-thaw cycles. *Constr. Build. Mater.* **2020**, *240*, 117947. [CrossRef]
25. Yan, Q.; Huang, P. Fractal Characteristic of Asphalt Mixture Void. *J. Tongji Univ.* **2004**, *32*, 43–48.
26. Thyagarajan, S.; Tashman, L.; Masad, E.; Bayomy, F. The heterogeneity and mechanical response of hot mix asphalt laboratory specimens. *Int. J. Pavement Eng.* **2010**, *11*, 107–121. [CrossRef]
27. Tan, Y.; Ren, J.; Ji, L.; Xu, Z. Analysis of influencing factors of the test precision of asphalt mixture voids based on X-ray CT. *J. Harbin Inst. Technol.* **2014**, *46*, 65–71.
28. Li, Z.; Tan, Y.; Wu, S.; Yang, F. The effects of the freeze-thaw cycle on the mechanical properties of the asphalt mixture. *J. Harbin Eng. Univ.* **2014**, *35*, 378–382.